Mathematics and Computers in Simulation 223 (2024) 158–170

Contents lists available at ScienceDirect

Mathematics and Computers in Simulation

journal homepage: www.elsevier.com/locate/matcom

Original articles

Non-uniform WENO-based quasi-interpolating splines from the Bernstein–Bézier representation and applications

F. Aràndiga [a], D. Barrera [b,*], S. Eddargani [c], M.J. Ibáñez [b], J.B. Roldán [d]

[a] Departament de Matemàtiques, Universitat de València (EG), Spain
[b] Department of Applied Mathematics, University of Granada, 18071 Granada, Spain
[c] Department of Mathematics, University of Rome Tor Vergata, 00133 Rome, Italy
[d] Department of Electronics and Computer Technology, University of Granada, 18071 Granada, Spain

ARTICLE INFO

Keywords:
Bernstein–Bézier representation
Quasi-interpolation
WENO

ABSTRACT

In this paper, we propose a family of C^1 non-uniform cubic quasi-interpolation schemes. The construction used here is mainly based on directly establishing the BB-coefficients by a suitable combination of the data values. These combinations generate masks for each of the BB-coefficients. These masks can contain free parameters, which allow us to write a quasi-interpolation schemes defined from a large stencil as a non-negative convex combination of others defined from sub-stencils of small sizes, which coincide with the concept of WENO, which we will use the deal with non-smooth data, or data with jumps. We consider an application of the proposed technique for real measured data related to memristors fabricated with hafnium oxide as a dielectric.

1. Introduction

Approximating data using splines is a common technique in numerical analysis and data interpolation. A spline is a piecewise-defined function that consists of polynomial segments joined together smoothly at specific points called knots.

Interpolation seeks a function that precisely aligns with specified data values, achieving an exact match that involves solving a linear system with as many unknowns as the spline space's dimension, but this approach is not suitable for efficient real-time processing of extensive data streams. Moreover, exact data point matching may be problematic, particularly when dealing with noisy data. From this point of view, local methods, such as spline quasi-interpolation, which do not need to solve any linear system, are advantageous. In fact, spline quasi-interpolation is a technique that involves fitting a spline to the data values without the requirement that the spline matches all the data values exactly, which makes it a useful technique for various types of data approximation problems. This technique was first introduced in a seminal works of Schoenberg [39,40] and referred to as smoothing interpolation.

A linear quasi-interpolation operator Q maps a function f to an element

$$Qf = \sum_{i=1}^{n} \phi(f, i) N_i,$$

of a suitable spline space, where n and N_i represent, the spline space dimension and function basis respectively, while $\phi(\bullet, i)$ are linear functionals. They can be defined in different ways, according to the provided information about the function f to be approximated.

* Corresponding author.
E-mail addresses: arandiga@uv.es (F. Aràndiga), dbarrera@ugr.es (D. Barrera), eddargani@mat.uniroma2.it (S. Eddargani), mibanez@ugr.es (M.J. Ibáñez), jroldan@ugr.es (J.B. Roldán).

https://doi.org/10.1016/j.matcom.2024.04.006
Received 10 December 2023; Received in revised form 23 March 2024; Accepted 8 April 2024
Available online 16 April 2024

Namely, they are point [15,38], derivative [13] or integral linear functionals [14,37]. In this work, we consider the first case, in which $\phi(f,i)$ is a finite linear combination of values of f. These functionals are defined in a such way that the spline Qf should reproduce polynomials and preferably functions in the given spline space, which guaranties a best approximation properties.

Moreover, the basis functions N_i, should meet some useful properties, such as, local support and non-negative partition of unity. Examples are Bernstein basis and any polynomial B-spline basis [31].

In this paper, we propose a family of quasi-interpolating splines in Bernstein–Bézier (BB-) form. The schemes are directly determined by fitting their Bernstein–Bézier (BB-) coefficients to an appropriate combination of the given data values. In particular, the BB-coefficients are calculated taking into account the required smoothness and polynomial accuracy. To each BB-coefficient, we will associate a mask of real values, this technique makes the construction fast and also gives more freedom in the construction. In general, we get masks with free parameters, which allows us to achieve more properties such as superconvergence and in many times to match the data values. This construction was first used to derive bivariate quasi-interpolation schemes defined on uniform three-direction triangulations (see [5,43]), Powell–Sabin triangulation [7], and a tensor product approximant [4]. A univariate study has been also developed in [6] for low degree splines.

Applying quasi-interpolation splines to non-smooth data, may lead to the Gibbs phenomenon, which is a phenomenon of oscillations or over- and under-shoots that occurs near discontinuities or sharp features in the data [12]. To avoid this limitation, one can adapt Essentially Non-Oscillatory (ENO) and Weighted-ENO (WENO) principles to spline quasi-interpolation for non-smooth data [2,18].

ENO and WENO are numerical methods that are primarily used in the context of solving hyperbolic partial differential equations and capturing shock waves accurately. The idea behind these approaches is to decompose the set of data values (stencil) used to define a functional $\phi(f,\ell)$ into a number of subsets (sub-stencils), and then define $\phi(f,\ell)$ only from the smooth subsets. The smoothness of a set of data values is measured by a smoothness indicator defined according to the type of data values [45].

The ENO technique uses only one sub-stencil from all available sub-stencils. In contrast, the WENO technique associates a real weight value to each sub-stencil and then uses all the sub-stencils to define the corresponding functional. The weights must be non-negative partition of unity [3,41].

We apply the WENO technique to the proposed quasi-interpolating spline schemes. And with the help of the free parameters in the masks defining the BB-coefficients, we can freely define the WENO weights. This allows us to obtain the appropriate weights or, more generally, to define the weights freely by imposing conditions on the free parameters.

The non-linear ENO and WENO techniques can directly interpolate data, offering a non-linear enhancement to traditional interpolation methods. For example, in [24], the authors introduced and evaluated fourth-order ENO and WENO schemes based on Lagrange interpolating operators, which have found useful application in radiative transfer problems [42].

Despite the widespread use of interpolation techniques, they often suffer from drawbacks, prompting the exploration of quasi-interpolating schemes, which offer certain advantages. The construction technique presented in this paper for quasi-interpolating schemes is explicit and does not require the construction of basis functions, making the schemes faster and more memory-efficient. Applying WENO and ENO techniques to these new schemes could prove more beneficial than applying them directly to Lagrange interpolation, offering enhanced performance and versatility in handling large data sets.

The non-linear improvement of the proposed quasi-interpolating spline schemes will be used in order to fit pulsed measurements performed in memristors based on a hafnium oxide dielectric. Memristors are electron devices that are intensively under scrutiny by the academia and industry [10,26,27]. These new and outstanding devices are promising in the electronic industry due to applications linked to non-volatile memories [23,27,28,32,44]. They have already been included in current industrial integrated circuits [26] and their market share with respect to the overall memory chip sales is expected to grow in the coming years. Among the memristors, resistive memories are the most important type. Because of the potential of these latter devices, they have been modelled and simulated from different perspectives. Modelling is important since the models (algebraic expressions that, in general, allow the calculation of charge and current as a function of the applied voltage) are incorporated in circuit simulators, so that designers can employ resistive memories to build new circuits that, among other components, include resistive memories, also known as RRAMs (Resistive Random Access Memories). There are different aspects of this discipline that have been tackled by our group, such as advanced statistical modelling [1,35] and compact modelling (for circuit simulation and design) [9,11,16,17,19,20,25,36]. In addition, in the parameter extraction facet, where a massive amount of experimental data is numerically analysed to extract physical constants that help in the modelling process, we have develop an important activity were advanced mathematical techniques were key to overcome the hurdles posed by noise and variability [8,21,22,30]. These numerical techniques lie upon state-of-the-art developments in the approximation theory that lead to smooth numerical derivatives through different methodologies, detection of straight lines and other issues making use of measurements that presents different types of noise. In what is related to parameter extraction, we have dealt so far with steady state measurements under ramped voltage stress, which is a usual operation regime in RRAMs. Nevertheless, operation in RRAMs is connected to input signals made of voltage pulses, as it is the case in memory devices, an essential application for the industry. Because of this, we focus the analysis of this manuscript in this operation regime and, as a consequence, we enter a new landscape from the mathematical viewpoint, since we are faced to the analysis and reconstruction of signals that present discontinuities and have non-uniform X-axis partitions. This latter issue is due to the measurement conditions, since the limitations of the measurement equipment produce unequal voltage steps, even if it is programmed to do so. Mathematically this measurement context leads us to a new paradigm from the numerical reconstruction perspective. In fact, the measured data features led us to use quasi-interpolating spline schemes in BB-form, as highlighted above, to accurately fit the measurements for modelling purposes.

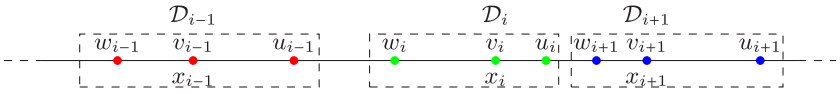

Fig. 1. Domain points.

The rest of paper is organized as follows: In Section 2, we introduce the notation used throughout the paper, as well as we construct a family of spline quasi-interpolation schemes on non-uniform partition. Section 3, is devoted to a WENO-based non-linear improvement of the presented schemes. In Section 4, we propose the use of WENO-based quasi-interpolation schemes in modelling experimental data obtained from resistive memories under a pulsed input voltage signals.

2. Non-uniform C^1-cubic quasi-interpolating splines

Throughout this paper, we consider a partition $X_n := \{a = x_0 < x_1 < \cdots < x_n = b\}$ of a bounded interval $I := [a, b]$. X_n divides I into $n \in \mathbb{N}$ sub-intervals $I_i := [x_i, x_{i+1}]$, $i = 0, \ldots, n-1$. The length of I_i is denoted by $h_i := x_{i+1} - x_i$. In the following, we consider the space of C^1 continuous cubic splines on X_n, defined by

$$S_3^1(X_n) = \left\{ s \in C^1(I) : \quad s_{|I_i} \in \mathbb{P}_3,\ i = 0, \ldots, n-1 \right\}.$$

In general, $\mathbb{P}_d$ will denote the linear space of polynomials of total degree less than or equal to d. Being the restriction $s_i := s_{|I_i}$ of a spline $s \in S_3^1(X_n)$ to the sub-interval I_i a polynomial in $\mathbb{P}_3$, it can be represented in BB-form on I_i. Therefore, there are coefficients $c_{k,i}$ such that

$$s_i(x) = \sum_{k=0}^{3} c_{k,i} B_k^i(x), \tag{1}$$

where $B_k^i(x) := B_k\left(\frac{x - x_i}{h_i}\right)$, with

$$B_k(x) := \frac{3!}{k!(3-k)!}(1-x)^{3-k}x^k, \quad x \in [0,1],$$

The Bernstein polynomials B_k, $k = 0, 1, 2, 3$, give a basis for $\mathbb{P}_3$ and form a partition of unity. The expression in (1) is said to be the BB-form of s_i, and the real coefficients $c_{k,i}$ are called the Bézier (B-) ordinates or BB-coefficients of s_i, which are linked to the domain points $p_{i,k} = \frac{3-k}{3}x_i + \frac{k}{3}x_{i+1}$.

We consider the union without repetitions of the domain points associated with all sub-intervals I_i, which yields the set $\mathcal{D} = \bigcup_{i\in\mathbb{Z}} \mathcal{D}_i$, where $\mathcal{D}_i := \{p_{i-1,2}, p_{i,0}, p_{i,1}\}$.

In order to simplify the notation, we use v_i, u_i and w_{i+1} to denote $p_{i,0}$, $p_{i,1}$, and $p_{i,2}$, respectively, then $\mathcal{D}_i = \{w_i, v_i, u_i\}$. Fig. 1 shows schematic representation of the domain point sets $\mathcal{D}_{i-1}$, $\mathcal{D}_i$, and $\mathcal{D}_{i+1}$.

Once the needed notations are introduced, we define a quasi-interpolating spline Qf that maps a function $f \in C(I)$ into an element of $S_3^1(X_n)$. Let values $f(x_i) =: f_i$, $i = 0, \ldots, n$, of a function f be given. Then Qf is defined by setting its B-ordinates on each sub-interval I_i induced by the partition X_n. More precisely, on the sub-interval I_i, the Qf is expressed as

$$Qf_{|I_i}(x) = V_i B_0^i(x) + U_i B_1^i(x) + W_{i+1} B_2^i + V_{i+1} B_3^i(x), \tag{2}$$

where V_i, U_i and W_i stand for the B-ordinates relative to the domain points v_i, u_i and w_i, respectively.

For each set of domain points $\mathcal{D}_i$ we associate a stencil, i.e, a set of discrete values of f. Namely, for the B-ordinates W_i, V_i, and U_i related to the domain points in $\mathcal{D}_i$ are computed from the values of f at the points in the stencil $S_i = \{x_{i-2}, x_{i-1}, x_i, x_{i+1}, x_{i+2}\}$, i.e., as linear combinations of the values in $f(S_i) = \{f_{i-2}, f_{i-1}, f_i, f_{i+1}, f_{i+2}\}$.

These B-ordinates determine the so-called masks,

$$W_i := \gamma_i \cdot f(S_i), \quad V_i := \beta_i \cdot f(S_i) \quad \text{and} \quad U_i := \alpha_i \cdot f(S_i), \tag{3}$$

where $\gamma_i := (\gamma_{i,-2}, \gamma_{i,-1}, \gamma_{i,0}, \gamma_{i,1}, \gamma_{i,2})$, $\beta_i := (\beta_{i,-2}, \beta_{i,-1}, \beta_{i,0}, \beta_{i,1}, \beta_{i,2})$, $\alpha_i := (\alpha_{i,-2}, \alpha_{i,-1}, \alpha_{i,0}, \alpha_{i,1}, \alpha_{i,2})$ are real vectors in $\mathbb{R}^5$, and $A \cdot B := \sum_{\ell=1}^{N} A_\ell\ B_\ell$ for $A = (A_1, \ldots, A_N)$ and $B = (B_1, \ldots, B_N)$.

The construction of Qf is then reduced to find the masks α_i, β_i and γ_i.

Problem 1. Find masks α_i, β_i and γ_i such that the quasi-interpolating spline Qf defined by (2) is C^1-continuous and $Qp = p$ for all $p \in \mathbb{P}_3$.

Before dealing with a solution of Problem 1, we need the following results concerning the relationship between C^1 smoothness at a knot x_i and the B-ordinates around x_i.

Proposition 1. *The quasi-interpolant defined by (2) is C^1-continuous at x_i if and only if*

$$\beta_{i,k} = \frac{1}{h_{i-1} + h_i}\left(h_i\gamma_{i,k} + h_{i-1}\alpha_{i,k}\right), \quad k = -2, -1, 0, 1, 2. \tag{4}$$

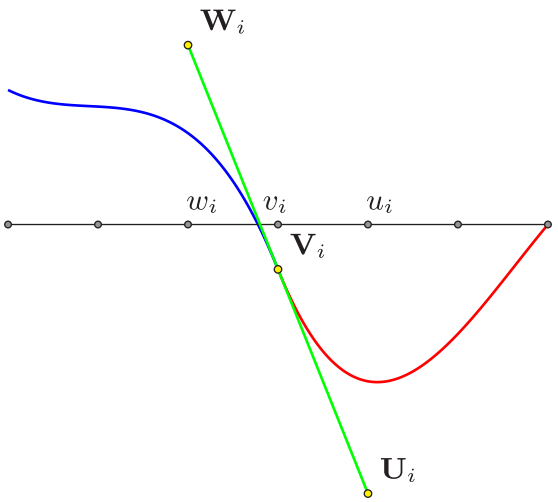

Fig. 2. C^1-smoothness condition at v_i.

Proof. Qf is C^1-continuous at x_i if and only if $Qf'_{|I_{i-1}}(x_i) = Qf'_{|I_i}(x_i)$, which is equivalent to control points $\mathbf{W}_i := (w_i, W_i)$, $\mathbf{V}_i := (v_i, V_i)$ and $\mathbf{U}_i := (u_i, U_i)$ being collinear. This holds if and only if

$$V_i = \frac{1}{h_{i-1}+h_i}\left(h_i W_i + h_{i-1} U_i\right),$$

and the claim follows. □

Fig. 2 illustrates an example of C^1-smoothness condition at v_i for a C^1-continuous spline.

Once the C^1-continuity has been characterized in terms of the masks, we must establish the conditions that ensures the exactness on $\mathbb{P}_3$ of the quasi-interpolation operator $Q : C^1(I) \longrightarrow C(I)$ defined as $Q[f] = Qf$. To this end, the B-ordinates of the monomials $m_k(x) := \left(\frac{x-v_i}{h}\right)^k$, $k = 0, 1, 2, 3$, are needed.

Lemma 2. *The B-ordinates of the restrictions to I_i of the monomials m_k are* $(1,1,1,1)$, $\left(0, \frac{1}{3}, \frac{2}{3}, 1\right)$, $\left(0, 0, \frac{1}{3}, 1\right)$ *and* $(0,0,0,1)$, *respectively.*

We are now in a position to provide a solution of Problem 1.

Proposition 3. *Problem 1 has infinitely many solutions depending for each $i = 0, \ldots, n$ on the two free parameters $\kappa_i = \alpha_{i,-2}$ and $\lambda_i = \beta_{i,-2}$.*

Proof. The B-ordinates V_i, U_i, W_{i+1} and V_{i+1} of Qf corresponding to the sub-interval I_i are given by (3). They should computed in such a way that they meet the C^1 smoothness conditions (4), as well as the exactness on $\mathbb{P}_3$. More precisely, the B-ordinates of Qm_k restricted to I_i must be equal to those of m_k. They are given in Lemma 2 and those of Qm_k, $k = 0, \ldots, 3$, are

$$\left(\sum_{k=-2}^{2}\beta_{i,k}, \sum_{k=-2}^{2}\alpha_{i,k}, \sum_{k=-2}^{2}\gamma_{i,k}, \sum_{k=-2}^{2}\beta_{i,k}\right),$$
$$\left(2\left(\beta_{i,2}-\beta_{i,-2}\right)+\beta_{i,1}-\beta_{i,-1}, 2\left(\alpha_{i,2}-\alpha_{i,-2}\right)+\alpha_{i,1}-\alpha_{i,-1}, -\gamma_{i,-2}+\gamma_{i,0}+2\gamma_{i,1}+3\gamma_{i,2}, -\beta_{i,-2}+\beta_{i,0}+2\beta_{i,1}\right.$$
$$\left.+3\beta_{i,2}\right),$$
$$\left(4\left(\beta_{i,2}+\beta_{i,-2}\right)+\beta_{i,-1}+\beta_{i,1}, 4\left(\alpha_{i,2}+\alpha_{i,-2}\right)+\alpha_{i,-1}+\alpha_{i,1}, \gamma_{i,-2}+\gamma_{i,0}+4\gamma_{i,1}+9\gamma_{i,2}, \beta_{i,-2}+\beta_{i,0}+4\beta_{i,1}+9\beta_{i,2}\right),$$
$$\left(8\left(\beta_{i,2}-\beta_{i,-2}\right)+\beta_{i,1}-\beta_{i,-1}, 8\left(\alpha_{i,2}-\alpha_{i,-2}\right)+\alpha_{i,1}-\alpha_{i,-1}, -\gamma_{i,-2}+\gamma_{i,0}+8\gamma_{i,1}+27\gamma_{i,2}, -\beta_{i,-2}+\beta_{i,0}+8\beta_{i,1}\right.$$
$$\left.+27\beta_{i,2}\right),$$

respectively. By equating the B-ordinates of m_k and Qm_k relative to I_i, we establish a linear system comprising 21 equations. Among these, five equations ensure C^1 smoothness, while the remainder pertain to the exactness on $\mathbb{P}_3$. With a rank of 13, this system falls short of the 15 unknowns, indicating the presence of infinitely many solutions. The general solution in the statement is determined using a Computer Algebra System. □

The choice $\kappa_i = \kappa$ and $\lambda_i = \lambda$ for all i leads to a 2-parametric family of quasi-interpolation operators $Q_{\lambda,\kappa}$. The explicit expressions of masks γ_i, β_i, and α_i are given next:

$$\gamma_{i,-2} = \frac{\lambda H_{i-1,1} - \kappa h_i}{h_{i-1}},$$

$$\gamma_{i,-1} = \frac{h_i\left(3\kappa H_{i-2,1}H_{i-2,2}H_{i-2,3}\right) - h_{i-1}h_iH_{i,1} - 3\lambda H_{i-2,1}H_{i-1,1}H_{i-2,2}H_{i-2,3}}{3h_{i-1}^2H_{i-1,1}H_{i-1,2}},$$

$$\gamma_{i,1} = \frac{h_i\left(3\kappa h_{i-2}H_{i-2,1}H_{i-2,3} + H_{i,1}h_{i-1}^2\right) - 3\lambda h_{i-2}H_{i-2,1}H_{i-1,1}H_{i-2,3}}{3h_{i-1}h_ih_{i+1}H_{i-1,1}},$$

$$\gamma_{i,2} = \frac{h_i\left(-3\kappa h_{i-2}H_{i-1,1}H_{i-2,2} - h_{i-1}^2h_i\right) + 3\lambda h_{i-2}H_{i-2,1}H_{i-1,1}H_{i-2,2}}{3h_{i-1}h_{i+1}H_{i,1}H_{i-1,2}},$$

$$\gamma_{i,0} = 1 - \gamma_{i,-2} - \gamma_{i,-1} - \gamma_{i,1} - \gamma_{i,2},$$

$$\beta_{i,-1} = -\lambda\frac{H_{i-2,1}H_{i-2,2}H_{i-2,3}}{h_{i-1}H_{i-1,1}H_{i-1,2}},$$

$$\beta_{i,0} = 1 + \lambda\frac{h_{i-2}H_{i-2,2}H_{i-2,3}}{h_{i-1}h_iH_{i,1}},$$

$$\beta_{i,1} = -\lambda\frac{h_{i-2}H_{i-2,1}H_{i-2,3}}{h_iH_{i-1,2}h_{i+1}},$$

$$\beta_{i,2} = \lambda\frac{h_{i-2}H_{i-2,1}H_{i-2,2}}{h_{i+1}H_{i,1}H_{i-1,2}},$$

$$\alpha_{i,-1} = \frac{h_{i-1}h_iH_{i,1} - 3\kappa H_{i-2,1}H_{i-2,2}H_{i-2,3}}{3h_{i-1}H_{i-1,1}H_{i-1,2}},$$

$$\alpha_{i,0} = \frac{3\kappa h_{i-2}H_{i-2,2}H_{i-2,3} + h_{i-1}\left(2h_iH_{i,1} + h_{i-1}\left(h_i + H_{i,1}\right)\right)}{3h_{i-1}h_iH_{i,1}},$$

$$\alpha_{i,1} = -\frac{3\kappa h_{i-2}H_{i-2,1}H_{i-2,3} + H_{i,1}h_{i-1}^2}{3h_iH_{i-1,1}h_{i+1}},$$

$$\alpha_{i,2} = \frac{3\kappa h_{i-2}H_{i-2,1}H_{i-2,2} + h_ih_{i-1}^2}{3h_{i+1}H_{i,1}H_{i-1,2}},$$

where $H_{j,1} := h_j + h_{j+1}$, $H_{j,2} := h_j + h_{j+1} + h_{j+2}$, $H_{j,3} := h_j + h_{j+1} + h_{j+2} + h_{j+3}$.

Remark 1. For a uniform partition, i.e. $h_i = h$, $i = 0, \dots, n-1$, the masks are

$$\alpha = \left(\kappa, -4\kappa - \frac{1}{9}, 6\kappa + \frac{5}{6}, \frac{1}{3} - 4\kappa, \kappa - \frac{1}{18}\right),$$
$$\beta = \{\lambda, -4\lambda, 6\lambda + 1, -4\lambda, \lambda\},$$
$$\gamma = \left(2\lambda - \kappa, -8\lambda + 4\kappa + \frac{1}{9}, 12\lambda - 6\kappa + \frac{7}{6}, -8\lambda + 4\kappa - \frac{1}{3}, 2\lambda - \kappa + \frac{1}{18}\right).$$

The following result holds.

Theorem 4. *We have*

1. $Q_{\kappa,\lambda}f$ *is* C^1.
2. $Q_{\kappa,\lambda}f = f$ *for all* $f \in \mathbb{P}_3$.
3. $\| Q_{\kappa,\lambda}f - f \| = \mathcal{O}(h^4)$ *for all* f *smooth, with* $h := \max_{0\le i\le n-1}\{h_i\}$.

Proof. The result follows as a consequence of Eq. (4), Lemma 2 and Proposition 3. □

The exactness on $\mathbb{P}_3$ makes $Q_{\kappa,\lambda}$ able to yield optimal approximation order for smooth functions. Fig. 3 shows examples of approximating discrete data by $Q_{\kappa,\lambda}$ for smooth data (left) and data with a jump (right). We observe that $Q_{\kappa,\lambda}$ generates over- and under-shots near the singularity point, i.e., Gibbs phenomena. In the next section, we propose a nonlinear modification of $Q_{\kappa,\lambda}$ based on WENO to handle non-smooth functions and avoid Gibbs phenomena.

3. Non-linear improvement of $Q_{\kappa,\lambda}$ based on WENO technique

This section is divided into three subsections. We will start by writing $Q_{\kappa,\lambda}f$ as a function of three quasi-interpolating splines of order 3, then of order 2, in the first two subsections, respectively. In the last subsection, we will provide a nonlinear improvement based on WENO technique.

3.1. Order 3

The B-ordinates corresponding to a set of domain points D_i are calculated from the values in a stencil S_i. One of these stencils may contain a jump value. Therefore, the WENO technique consists in dividing a stencil into a number of small sub-stencils. In our case,

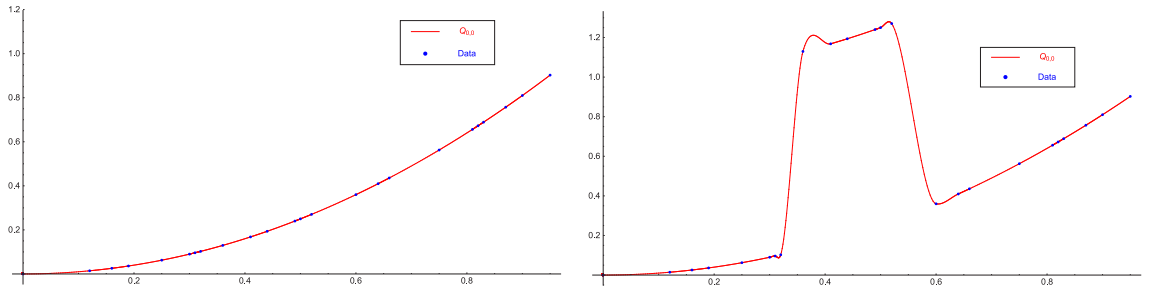

Fig. 3. Approximation by $Q_{0,0}$, smooth data (left), and non-smooth data (right).

the stencil S_i is divided into three small stencils, namely $S_{i,1} := \{f_{i-2}, f_{i-1}, f_i\}$, $S_{i,2} := \{f_{i-1}, f_i, f_{i+1}\}$, and $S_{i,3} := \{f_i, f_{i+1}, f_{i+2}\}$. Then we try to use data values only in the smooth sub-stencils.

For each stencil $S_{i,j}$, $j = 1, 2, 3$, we associate a smoothness indicator, marked by $IS_{i,j}$ and defined according to the characteristics of the data to be approximated.

From each sub-stencil $S_{i,j}$, $j = 1, 2, 3$, we define a quasi-interpolating spline $Q_j f$.

Problem 2. Determine masks $\alpha^2_{i,j} := \left(\alpha^2_{i,j,-1}, \alpha^2_{i,j,0}, \alpha^2_{i,j,1}\right)$, $\beta^2_{i,j} := \left(\beta^2_{i,j,-1}, \beta^2_{i,j,0}, \beta^2_{i,j,1}\right)$ and $\gamma^2_{i,j} := \left(\gamma^2_{i,j,-1}, \gamma^2_{i,j,0}, \gamma^2_{i,j,1}\right)$, $j = 1, 2, 3$, such that the quasi-interpolating splines $Q^2_j f$, $j = 1, 2, 3$, defined on each sub-interval I_i as

$$Q^2_j f_{|I_i} = V^2_{i,j} B^i_0 + W^2_{i,j} B^i_1 + U^2_{i+1,j} B^i_2 + V^2_{i+1,j} B^i_3$$

with

$$U^2_{i,j} = \alpha^2_{i,j} \cdot f\left(S_{i,j}\right), \quad V^2_{i,j} = \beta^2_{i,j} \cdot f\left(S_{i,j}\right), \quad W^2_{i,j} = \gamma^2_{i,j} \cdot f\left(S_{i,j}\right),$$

are C^1 continuous and $Q^2_j p = p$ for all $p \in \mathbb{P}_2$.

The following result shows that this problem has a unique solution.

Proposition 5. *For $j = 1$, Problem 2 has a unique solution, with masks $\alpha^2_{i,1}$, $\beta^2_{i,1}$ and $\gamma^2_{i,1}$ given by*

$$\alpha^2_{i,1} = \left(-\frac{h^2_{i-1}}{3h_{i-2}H_{i-2,1}}, \frac{H_{i-2,1}}{3h_{i-2}}, \frac{h_{i-2} + H_{i-2.1}}{3H_{i-2,1}}\right),$$
$$\beta^2_{i,1} = (0, 0, 1),$$
$$\gamma^2_{i,1} = \left(\frac{h_{i-1}h_i}{3h_{i-2}H_{i-2,1}}, -\frac{H_{i-2,1}h_i}{3h_{i-2}h_{i-1}}, 1 + \frac{h_i\left(h_{i-1} + H_{i-2,1}\right)}{3h_{i-1}H_{i-2,1}}\right).$$

Proof. The quasi-interpolating spline $Q^2_1 f$ is C^1-continuous at x_i if and only if

$$\beta_{i,1,\ell} = \frac{1}{H_{i-1,1}}\left(\gamma_{i,1,\ell}h_{i-1} + \alpha_{i,1,\ell}h_i\right), \quad \ell = -1, 0, 1.$$

The exactness of $Q^2_1 f$ on quadratic polynomials is equivalent to the following conditions:

$$\alpha_{i,1,-1} + \alpha_{i,1,0} + \alpha_{i,1,1} - 1 = 0, \beta_{i,1,-1} + \beta_{i,1,0} + \beta_{i,1,1} - 1 = 0, \gamma_{i,1,-1} + \gamma_{i,1,0} + \gamma_{i,1,1} - 1 = 0,$$
$$\left(-\alpha_{i,1,-1} - \alpha_{i,1,0} + \frac{1}{3}\right)h_{i-1} - \alpha_{i,1,-1}h_{i-2} = 0, \beta_{i,1,-1}\left(-h_{i-2}\right) - \left(\beta_{i,1,-1} + \beta_{i,1,0}\right)h_{i-1} = 0,$$
$$-\gamma_{i,1,-1}h_{i-2} - \left(\gamma_{i,1,-1} + \gamma_{i,1,0}\right)h_{i-1} - \frac{h_i}{3} = 0, \alpha_{i,1,0}h^2_{i-1} + \alpha_{i,1,-1}\left(h_{i-2} + h_{i-1}\right)^2 = 0,$$
$$\beta_{i,1,0}h^2_{i-1} + \beta_{i,1,-1}\left(h_{i-2} + h_{i-1}\right)^2 = 0, \gamma_{i,1,0}h^2_{i-1} + \gamma_{i,1,-1}\left(h_{i-2} + h_{i-1}\right)^2 = 0.$$

This yields a linear system of twelve equations with nine unknowns. The system rank, equal to nine, indicates that there are only nine independent equations, thereby resulting in a unique solution. □

Now, we provide the values of the masks corresponding to the quasi-interpolating splines $Q^2_2 f$ and $Q^2_3 f$.

Proposition 6. *The masks*

$$\alpha^2_{i,2} = \left(\frac{h_i}{3H_{i-1,1}}, \frac{H_{i-1,1} + h_i}{3h_i}, -\frac{h^2_{i-1}}{3h_i H_{i-1,1}}\right),$$

$$\beta_{i,2}^2 = (0,1,0)\,,$$
$$\gamma_{i,2}^2 = \left(-\frac{h_i^2}{3h_{i-1}H_{i-1,1}}, \frac{h_{i-1}+H_{i-1,1}}{3h_{i-1}}, \frac{h_{i-1}}{3H_{i-1,1}} \right),$$

and

$$\alpha_{i,3}^2 = \left(1 + \frac{\left(h_i + H_{i,1}\right) h_{i-1}}{3H_{i,1}h_i}, -\frac{h_{i-1}H_{i,1}}{3h_ih_{i+1}}, \frac{h_{i-1}h_i}{3h_{i+1}H_{i,1}} \right),$$
$$\beta_{i,3}^2 = (1,0,0)\,,$$
$$\gamma_{i,3}^2 = \left(\frac{H_{i,1}+h_{i+1}}{3H_{i,1}}, \frac{H_{i,1}}{3h_{i+1}}, -\frac{h_i^2}{3h_{i+1}H_{i,1}} \right),$$

produce respectively the unique quasi-interpolating splines $Q_2 f$ and $Q_3 f$, such that

$$Q_j^2 p = p \quad \textit{for all} \quad p \in \mathbb{P}_2 \quad \textit{and} \quad Q_j^2 f \in C^1(I), \quad j = 2,3.$$

Proof. The proof runs as in Proposition 5. □

As a consequence of Propositions 5 and 6, the following result holds.

Theorem 7. *For $j = 1,2,3$,*

(1) $Q_j^2 f$ is $C^1(I)$.
(2) $Q_j^2 p = p$ for all $p \in \mathbb{P}_2$.
(3) $\| Q_j^2 f - f \| = \mathcal{O}(h^3)$ for a smooth function f.

In order to apply WENO technique, we need to write $Q_{\kappa,\lambda} f$ as non-negative convex combination of $Q_j^2 f$, $j = 1,2,3$. Namely,

$$Q_{\kappa,\lambda} f_{|I_i} = \tau_{i,1} Q_1^2 f_{|I_i} + \tau_{i,2} Q_2^2 f_{|I_i} + \left(1 - \tau_{i,1} - \tau_{i,2}\right) Q_3^2 f_{|I_i}, \quad \tau_{i,1}, \tau_{i,2} \geq 0. \tag{5}$$

This will not always be possible.

Proposition 8. *Eq. (5) has a solution if and only if $\lambda = 0$, and then*

$$\tau_{i,1} = -\frac{3\kappa_i h_{i-2} H_{i-2,1}}{h_{i-1}^2},$$
$$\tau_{i,2} = \frac{h_{i-1}^2 h_i H_{i.1} - 3\kappa_i h_{i-2} H_{i-2,1}\left(h_{i-1}H_{i-2,1} - h_i H_{i,1}\right)}{h_{i-1}^2 h_i H_{i-1,2}}.$$

The value of κ should be chosen so that $0 \leq \tau_{i,1},\ \tau_{i,2} \leq 1$. For instance, for uniform partition and $\kappa = -\frac{1}{36}$, it yields

$$Q_{-1/36,0} f = \frac{1}{6}\left(Q_1^2 f + 4Q_2^2 f + Q_3^2 f\right).$$

In order to get more freedom in the choice of convex weights to write $Q_{\kappa,\lambda}$ as a function of low-order quasi-interpolating splines, we reduce the order of convergence from three to two, imposing accuracy only on $\mathbb{P}_1$.

3.2. Order 2

In this subsection, we follow the same strategy used above. That is, we consider the same partition of S_i into the three sub-stencils $S_{i,j}$, $j = 1,2,3$, and then define local quasi-interpolating splines corresponding to each stencil. Accuracy will be imposed only on linear polynomials, which will generate masks with free parameters.

Problem 3. Determine masks $\alpha_{i,j}^1 := \left(\alpha_{i,j,-1}^1, \alpha_{i,j,0}^1, \alpha_{i,j,1}^1\right)$, $\beta_{i,j}^1 := \left(\beta_{i,j,-1}^1, \beta_{i,j,0}^1, \beta_{i,j,1}^1\right)$ and $\gamma_{i,j}^1 := \left(\gamma_{i,j,-1}^1, \gamma_{i,j,0}^1, \gamma_{i,j,1}^1\right)$, $j = 1,2,3$, such that the quasi-interpolating splines $Q_j^1 f$, $j = 1,2,3$, defined on each sub-interval I_i as

$$Q_j^1 f_{|I_i} = V_{i,j}^1 B_0^i + W_{i,j}^1 B_1^i + U_{i+1,j}^1 B_2^i + V_{i+1,j}^1 B_3^i$$

with

$$U_{i,j}^1 = \alpha_{i,j}^1 \cdot f\left(S_{i,j}\right), \quad V_{i,j}^1 = \beta_{i,j}^1 \cdot f\left(S_{i,j}\right), \quad W_{i,j}^1 = \gamma_{i,j}^2 \cdot f\left(S_{i,j}\right),$$

are C^1 continuous and $Q_j^1 p = p$ for all $p \in \mathbb{P}_1$.

Problem 3 has infinitely many solutions. Keep in mind that the main target is to write

$$Q_{\kappa,\lambda} f_{|I_i} = \widetilde{\tau}_{i,1} Q_1^1 f_{|I_i} + \widetilde{\tau}_{i,2} Q_2^1 f_{|I_i} + \left(1 - \widetilde{\tau}_{i,1} - \widetilde{\tau}_{i,2}\right) Q_3^1 f_{|I_i}, \quad \widetilde{\tau}_{i,1}, \widetilde{\tau}_{i,2} \geq 0. \tag{6}$$

Proposition 9. *For $j = 1$, Problem 3 has an infinite number of solutions depending on two parameters $\alpha^1_{i,1,-1} = \kappa_{i,1}$ and $\beta^1_{i,1,-1} = \lambda_{i,1}$. The masks are given by*

$$\alpha^1_{i,1} = \left(\kappa_{i,1}, \kappa_{i,1}\left(-\frac{h_{i-2}}{h_{i-1}} - 1\right) + \frac{1}{3}, \frac{\kappa_{i,1}h_{i-2}}{h_{i-1}} + \frac{2}{3}\right),$$
$$\beta^1_{i,1} = \left(\lambda_{i,1}, -\frac{H_{i-2,1}\lambda_{i,1}}{h_{i-1}}, \frac{h_{i-2}\lambda_{i,1}}{h_{i-1}} + 1\right),$$
$$\gamma^1_{i,1} = \left(\frac{h_i\left(\lambda_{i,1} - \kappa_{i,1}\right)}{h_{i-1}} + \lambda_{i,1}, -\frac{-3H_{i-2,1}h_i\kappa_{i,1} + 3H_{i-2,1}H_{i-1,1}\lambda_{i,1} + h_{i-1}h_i}{3h^2_{i-1}},\right.$$
$$\left.\frac{h_i\left(h_{i-1} - 3h_{i-2}\kappa_{i,1}\right) + 3h_{i-2}H_{i-1,1}\lambda_{i,1}}{3h^2_{i-1}} + 1\right).$$

Proof. The proof runs as in Proposition 5. The C^1-smoothness conditions reduced to the following three equations:

$$\beta_{i,1,\ell} = \frac{1}{H_{i-1,1}}\left(\gamma_{i,1,\ell}h_{i-1} + \alpha_{i,1,\ell}h_i\right), \quad \ell = -1, 0, 1.$$

$Q^1_1 f$ is exact on linear polynomials if and only if

$$\alpha_{i,1,-1} + \alpha_{i,1,0} + \alpha_{i,1,1} - 1 = 0, \beta_{i,1,-1} + \beta_{i,1,0} + \beta_{i,1,1} - 1 = 0, \gamma_{i,1,-1} + \gamma_{i,1,0} + \gamma_{i,1,1} - 1 = 0,$$
$$\left(-\alpha_{i,1,-1} - \alpha_{i,1,0} + \frac{1}{3}\right)h_{i-1} - \alpha_{i,1,-1}h_{i-2} = 0, \beta_{i,1,-1}\left(-h_{i-2}\right) - \left(\beta_{i,1,-1} + \beta_{i,1,0}\right)h_{i-1} = 0,$$
$$-\gamma_{i,1,-1}h_{i-2} - \left(\gamma_{i,1,-1} + \gamma_{i,1,0}\right)h_{i-1} - \frac{h_i}{3} = 0.$$

This leads to a linear system of nine equations with nine unknowns. The rank of this system equals seven, indicating an infinite number of solutions. This confirms the claim. □

By the same, we can compute the masks associated with the operators Q^1_2 and Q^1_3.

Proposition 10. *The masks producing the quasi-interpolating splines $Q^1_2 f$ and $Q^1_3 f$ are as follows: for $j = 2$*

$$\alpha^2_{i,1} = \left(\kappa_{i,2}, \frac{-3\kappa_{i,2}H_{i-1,1} + h_{i-1} + 3h_i}{3h_i}, \frac{\left(3\alpha_{i-1} - 1\right)h_{i-1}}{3h_i}\right),$$
$$\beta^2_{i,1} = \left(\lambda_{i,2}, 1 - \frac{\lambda_{i,2}H_{i-1,1}}{h_i}, \frac{\lambda_{i,2}h_{i-1}}{h_i}\right),$$
$$\gamma^2_{i,1} = \left(\lambda_{i,2} + \frac{h_i\left(\lambda_{i,2} - \kappa_{i,2}\right)}{h_{i-1}}, \kappa_{i,2}\left(\frac{h_i}{h_{i-1}} + 1\right) - \frac{\lambda_{i,2}H^2_{i-1,1}}{h_{i-1}h_i} + \frac{2}{3}, -\kappa_{i,2} + \lambda_{i,2}\left(\frac{h_{i-1}}{h_i} + 1\right) + \frac{1}{3}\right),$$

and, for $j = 3$,

$$\alpha^3_{i,1} = \left(\frac{3\kappa_{i,3}h_i + h_{i-1} + 3h_i}{3h_i}, -\frac{3\kappa_{i,3}H_{i,1} + h_{i-1}}{3h_i}, \kappa_{i,3}\right),$$
$$\beta^3_{i,1} = \left(1 - \frac{\lambda_{i,3}h_i}{H_{i,1}}, \lambda_{i,3}, -\frac{\lambda_{i,3}h_i}{H_{i,1}}\right),$$
$$\gamma^3_{i,1} = \left(-\frac{h_i\left(\kappa_{i,3}H_{i,1} + \lambda_{i,3}H_{i-1,1}\right)}{h_{i-1}H_{i,1}} + \frac{2}{3}, \frac{3\kappa_{i,3}H_{i,1} + 3\lambda_{i,3}H_{i-1,1} + h_{i-1}}{3h_{i-1}}, \frac{h_i\left(\kappa_{i,3} - H_{i,1} - \lambda_{i,3}H_{i-1,1}\right)}{h_{i-1}H_{i,1}}\right),$$

where $\kappa_{i,\ell}$ and $\lambda_{i,\ell}$, $\ell = 2, 3$, are free parameters.

Again, and as a consequence of the previous results, it holds

Theorem 11. *For $j = 1, 2, 3$,*

(1) $Q^1_j f$ is $C^1(I)$.
(2) $Q^1_j p = p$ for all $p \in \mathbb{P}_1$.
(3) $\| Q^1_j f - f \| = \mathcal{O}(h^2)$ for a smooth function f.

The free parameters should chosen carefully. In our case they should chosen such that the weights $\widetilde{\tau}_{i,\ell}$, $\ell = 1, 2$, involved in (6) are non-negative and meet $\widetilde{\tau}_{i,1} + \widetilde{\tau}_{i,2} < 1$.

For instance, we have

- $\widetilde{\tau}_{i,1} = \widetilde{\tau}_{i,2} = 1/3$, if and only if

$$\lambda_{i,1} = \lambda,\ \kappa_{i,1} = 3\kappa,\ \lambda_{i,2} = -\frac{3h_{i-2}H_{i-2,1}\left(h_{i-2} + 2H_{i-1,1} + h_i\right)\lambda}{h_{i-1}H_{i-1,1}H_{i-1,2}},$$

$$\kappa_{i,2} = -\frac{9h_{i-2}H_{i-2,1}\left(h_{i-2}+2H_{i-1,1}+h_{i+1}\right)\kappa + h_{i-1}\left(h_{i-1}^2+\left(2h_i+h_{i+1}\right)h_{i-1}-2h_iH_{i,1}\right)}{3h_{i-1}H_{i-1,1}H_{i-1,2}},$$
$$\lambda_{i,3} = -\frac{3h_{i-2}H_{i-2,1}H_{i-2,2}\lambda}{h_ih_{i+1}H_{i-1,2}},\ \kappa_{i,3} = \frac{3h_{i-2}H_{i-2,1}H_{i-2,2}\kappa + h_ih_{i-1}^2}{h_{i+1}H_{i,1}H_{i-1,2}}.$$

- $\widetilde{\tau}_{i,1} = 1/4$, $\widetilde{\tau}_{i,2} = 1/2$, if and only if

$$\lambda_{i,1} = 4\lambda,\ \kappa_{i,1} = 4\kappa,\ \lambda_{i,2} = -\frac{2h_{i-2}H_{i-2,1}\left(h_{i-2}+2H_{i-1,2}\right)\lambda}{h_{i-1}H_{i-1,1}H_{i-1,2}},$$
$$\kappa_{i,2} = -\frac{12h_{i-2}H_{i-2,1}\left(h_{i-2}+2H_{i-1,2}\right)\kappa + h_{i-1}\left(h_{i-1}^2+\left(2h_i+h_{i+1}\right)h_{i-1}-3h_iH_{i-1,1}\right)}{6h_{i-1}H_{i-1,1}H_{i-1,2}},$$
$$\lambda_{i,3} = -\frac{4h_{i-2}H_{i-2,1}H_{i-2,2}\lambda}{h_ih_{i+1}H_{i-1,2}},\ \kappa_{i,3} = \frac{12h_{i-2}H_{i-2,1}H_{i-2,2}\kappa + 4h_ih_{i-1}^2}{3h_{i+1}H_{i,1}H_{i-1,2}}.$$

- $\widetilde{\tau}_{i,1} = 1/6$, $\widetilde{\tau}_{i,2} = 2/3$, if and only if

$$\lambda_{i,1} = 6\lambda,\ \kappa_{i,1} = 6\kappa,\ \lambda_{i,2} = -\frac{3h_{i-2}H_{i-2,1}\left(h_{i-2}+2H_{i-1,1}+h_{i+1}\right)\lambda}{2h_{i-1}H_{i-1,1}H_{i-1,2}},$$
$$\kappa_{i,2} = -\frac{18h_{i-2}H_{i-2,1}\left(h_{i-2}+2H_{i-1,1}+h_{i+1}\right)\kappa + h_{i-1}\left(h_{i-1}^2+\left(2h_i+h_{i+1}\right)h_{i-1}-5h_iH_{i,1}\right)}{12h_{i-1}H_{i-1,1}H_{i-1,2}},$$
$$\lambda_{i,3} = -\frac{6h_{i-2}H_{i-2,1}H_{i-2,2}\lambda}{h_ih_{i+1}H_{i-1,2}},\ \kappa_{i,3} = \frac{6h_{i-2}H_{i-2,1}H_{i-2,2}\kappa + 2h_ih_{i-1}^2}{h_{i+1}H_{i,1}H_{i-1,2}}.$$

In summary, $Q_{\kappa,\lambda}$ can be written as a non-negative convex combination of three quasi-interpolation operators reproducing quadratic polynomials for $\lambda = 0$, and as a non-negative convex combination of three quasi-interpolation operators exact on linear polynomials for any real coefficient λ and κ. These two results will be used below to derive non-negative weights for the WENO technique.

3.3. WENO technique

A WENO-based quasi-interpolating spline $Q_{\kappa,\lambda}^{\omega,\ell}f$ is defined as

$$Q_{\kappa,\lambda}^{\omega,\ell}f_{|I_i}(x) = V_i^{\omega,\ell}B_0^i(x) + W_i^{\omega,\ell}B_1^i(x) + U_{i+1}^{\omega,\ell}B_2^i(x) + V_{i+1}^{\omega,\ell}B_3^i(x),$$

with

$$U_i^{\omega,\ell} := \omega_{i,1}^\ell U_{i,1}^\ell + \omega_{i,2}^\ell U_{i,2}^\ell + \omega_{i,3}^\ell U_{i,3}^\ell,$$
$$V_i^{\omega,\ell} := \omega_{i,1}^\ell V_{i,1}^\ell + \omega_{i,2}^\ell V_{i,2}^\ell + \omega_{i,3}^\ell V_{i,3}^\ell,$$
$$W_i^{\omega,\ell} := \omega_{i,1}^\ell W_{i,1}^\ell + \omega_{i,2}^\ell W_{i,2}^\ell + \omega_{i,3}^\ell W_{i,3}^\ell.$$

For $\ell = 2$, the parameter λ must be zero, as well as the weights $\omega_{i,j}^2$, $j = 1,2,3$, must be chosen so that if f is smooth, then $\omega_{i,1}^2 \approx \frac{1}{6}$, $\omega_{i,2}^2 \approx \frac{4}{6}$, $\omega_{i,3}^2 \approx \frac{1}{6}$ and $Q_{\kappa,0}^{\omega,2}f_{|I_i} \approx Q_{\kappa,0}f_{|I_i}$.

Similarly, we should have $\omega_{i,j}^1 \approx \widetilde{\tau}_{i,j}$ and $Q_{\kappa,\lambda}^{\omega,1}f_{|I_i} \approx Q_{\kappa,\lambda}f_{|I_i}$ for a smooth function f. On the other hand, if f has a jump at a point in $\left(x_i, x_{i+1}\right]$ (e.g. in the stencils $S_{i,2}$ and $S_{i,3}$), then $\omega_{i,1}^\ell \approx 1$ and $\omega_{i,2}^\ell \approx \omega_{i,3}^\ell \approx 0$, so $Q_{\kappa,\lambda}^{\omega,\ell}f_{|I_i} \approx Q_1^\ell f_{|I_i}$ keeping the properties of Q_1^ℓ. To this end, we define,

$$\xi_{i,1}^2 := \frac{1}{6\left(\varepsilon + IS_{i,1}\right)^2},\quad \xi_{i,2}^2 := \frac{4}{6\left(\varepsilon + IS_{i,2}\right)^2},\quad \xi_{i,3}^2 := \frac{1}{6\left(\varepsilon + IS_{i,3}\right)^2},$$
$$\xi_{i,1}^1 := \frac{\widetilde{\tau}_{i,1}}{\left(\varepsilon + IS_{i,1}\right)^2},\quad \xi_{i,2}^1 := \frac{\widetilde{\tau}_{i,2}}{\left(\varepsilon + IS_{i,2}\right)^2},\quad \xi_{i,3}^1 := \frac{\widetilde{\tau}_{i,3}}{\left(\varepsilon + IS_{i,3}\right)^2},$$

where the smoothness indicators $IS_{i,k}$ are properly chosen according to the problem to be addressed, and the weights $\omega_{i,j}^\ell$ are defined as

$$\omega_{i,j}^\ell := \frac{\xi_{i,j}^\ell}{\xi_{i,1}^\ell + \xi_{i,2}^\ell + \xi_{i,3}^\ell}.$$

The parameter ε is a non-negative real value used to avoid zero in the denominator.

This construction leads to the following result.

Theorem 12. *For $\ell = 1,2$, we have, if f is smooth*

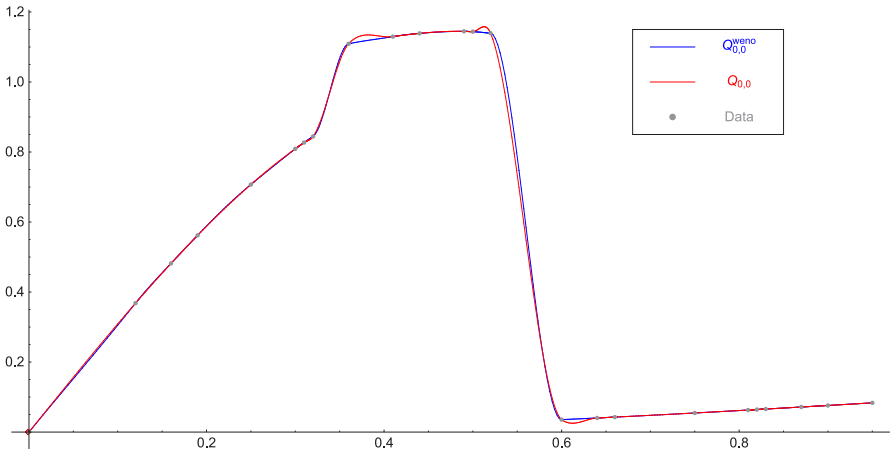

Fig. 4. Reconstruction with $Q^{\omega,1}_{0,0}$ (blue) and $Q_{0,0}$ (red). (For interpretation of the references to colour in this figure legend, the reader is referred to the web version of this article.)

- $Q^{\omega,\ell}_{\kappa,\lambda} f$ *is* C^1.
- $Q^{\omega,\ell}_{\kappa,\lambda} f = f$ *for all* $f \in \mathbb{P}_\ell$.
- $\| Q^{\omega,\ell}_{\kappa,\lambda} f - f \| = \mathcal{O}(h^4)$.

and if f *has a discontinuity jump at* (x_{i-1}, x_i) *then*

- $Q^{\omega,\ell}_{\kappa,\lambda} f$ *is* C^1
- $\| Q^{\omega,\ell}_{\kappa,\lambda} f - f \|_{[x_i,+\infty)} = \mathcal{O}(h^{\ell+1})$.

Proof. In both cases, $Q^{\omega,\ell}_{\kappa,\lambda} f$ is C^1-continuous, since is just a combination of three C^1-smooth operators. Moreover,

$$\begin{aligned} \| Q^{\omega,\ell}_{\kappa,\lambda} f - f \| &= \| Q^{\omega,\ell}_{\kappa,\lambda} f - Q_{\kappa,\lambda} f + Q_{\kappa,\lambda} f - f \| \\ &\leq \| Q^{\omega,\ell}_{\kappa,\lambda} f - Q_{\kappa,\lambda} f \| + \| Q_{\kappa,\lambda} f - f \| . \end{aligned}$$

By construction, if f is smooth, then $\| Q^{\omega,\ell}_{\kappa,\lambda} f - Q_{\kappa,\lambda} f \| = \mathcal{O}(h^4)$, and by Theorem 4, we have $\| Q_{\kappa,\lambda} f - f \| = \mathcal{O}(h^4)$, which proves that $\| Q^{\omega,\ell}_{\kappa,\lambda} f - f \| = \mathcal{O}(h^4)$.

However, this not guaranties that $Q^{\omega,\ell}_{\kappa,\lambda} p = p$, $p \in \mathbb{P}_\ell$. Although, the operator $Q^{\omega,\ell}_{\kappa,\lambda}$ is a combination of three operator that are exact on $\mathbb{P}_\ell$, which proves the statements in the case that f is smooth.

If f has a jump at $\bar{x} \in [x_{i-1}, x_i]$, then the BB-coefficients related to the intervals I_{i+j}, $j = -2, -1, 0, 1$, will be affected. Namely, at maximum two weights should be ≈ 0, and then

$$\| Q^{\omega,\ell}_{\kappa,\lambda} - Q_{\kappa,\lambda} \| = \max \left\{ \| Q^\ell_1 - Q_{\kappa,\lambda} \|, \| Q^\ell_2 - Q_{\kappa,\lambda} \|, \| Q^\ell_3 - Q_{\kappa,\lambda} \| \right\}.$$

Moreover, $\| Q^\ell_j - Q_{\kappa,\lambda} \| = \mathcal{O}(h^{\ell+1})$, $j = 1, 2, 3$, which concludes the proof. □

In Fig. 4 we illustrate the result obtained by applying the operator $Q^{\omega,1}_{0,0}$ and $Q_{0,0}$ to non-smooth data values. It is clear that with WENO technique, we obviously avoid the Gibbs phenomena, as well as we reach the optimal order in the smooth region.

4. Fitting pulsed measurements performed in memristors based on a hafnium oxide dielectric

The devices measured are based on the TiN/Ti/HfO_2/W stack. A (200 nm TiN/10 nm Ti) bi-layer is used as top electrode, and for the bottom electrode, a layer 50 nm-thick of W was employed [29,30]. The oxide was a 10 nm-thick HfO_2 layer grown by atomic layer deposition [34]. For the measurements, we used the Keysight B1500A semiconductor parameter analyser connected to a probe station (Karl Suss PSM6). The measuring unit was the B1530 module. It consists of a waveform generator and fast measurement unit (WGFMU) that works fine for pulsed signals. The bottom electrode was grounded and the input voltage was applied to the top electrode. Different pulsed signals were employed with pulse widths variating from milliseconds to hundreds of nanoseconds. The device current was measured; due to the pulsed and, obviously, non-continuous nature of the input, this current was also discontinuous.

The usual representation for modelling in these devices is based on current versus voltage curves. Nevertheless, it is also used the charge versus flux approach [8,33]. Given the current $i(t)$, the charge can be calculated as

$$Q(t) = \int_0^t i(\tau)\, d\tau,$$

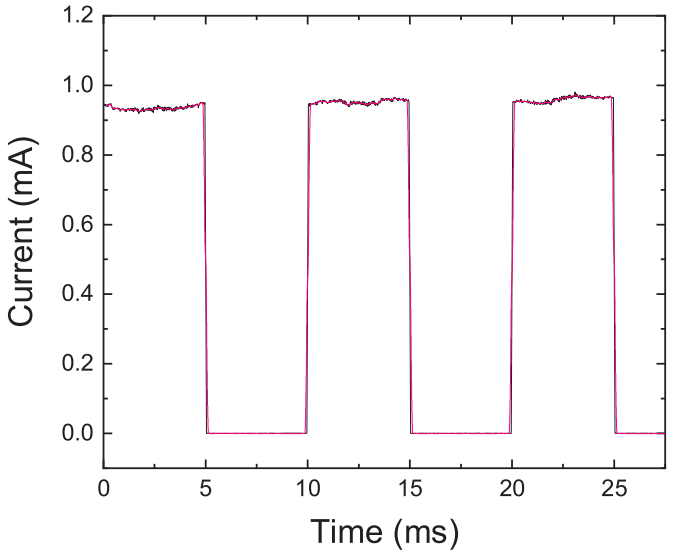

Fig. 5. Current data (black) and WENO quasi-interpolant.

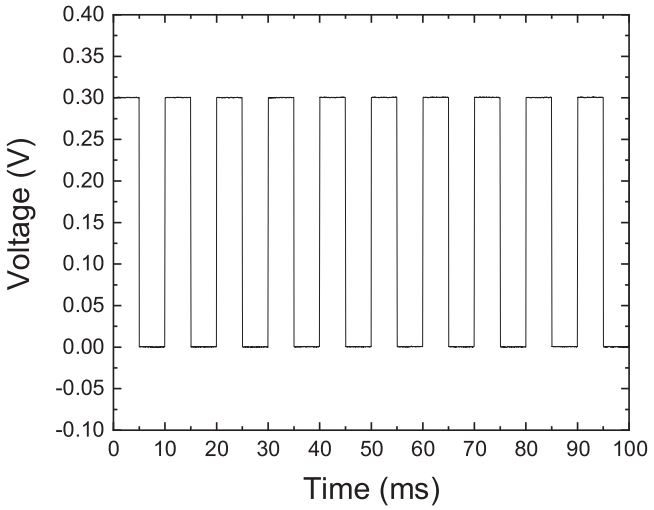

Fig. 6. Voltage data.

while, from the voltage $v(t)$, the flux is obtained with

$$\phi(t) = \int_0^t v(\tau)\, d\tau.$$

For the charge calculation the current accurate approximation as a function of time is needed. The measurement features makes the X axis knot set a non-uniform distribution. The approximation methodology described in the previous sections allows a feasible approximation of the current versus time data. Therefore, the charge calculation can be easily done.

Fig. 5 shows the current data for which the charge will be computed, as well as the corresponding WENO quasi-interpolant. The voltage data are shown in Fig. 6.

The following indicators have been used:

$$IS_{i,1} = 10^4 \left(f_{i-2} - 2f_{i-1} + f_i\right)^6,$$
$$IS_{i,2} = 10^4 \left(f_{i-1} - 2f_i + f_{i+1}\right)^6,$$
$$IS_{i,3} = 10^4 \left(f_i - 2f_{i+1} + f_{i+2}\right)^6.$$

The factor "10^4" is included to deal with the very small values resulting from the analysed device.

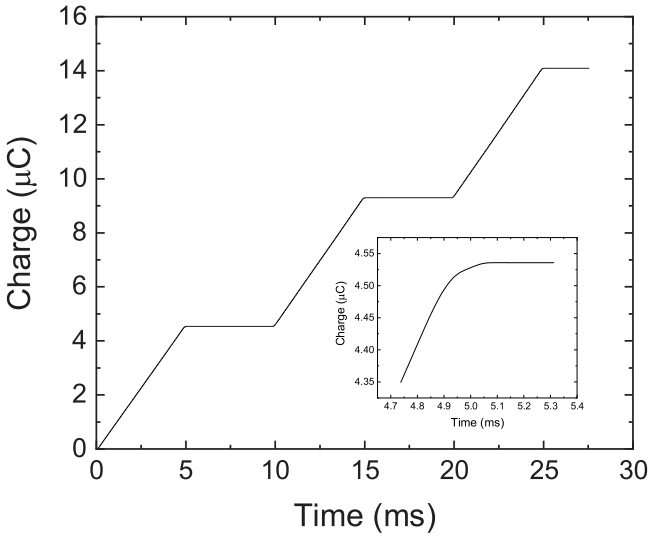

Fig. 7. Charge versus time, calculated by integrating the current versus time data.

Finally, the computed charge is shown versus time in Fig. 7. It contains a small plot illustrating the smoothness of the charge versus time in a neighbourhood of a current discontinuity point. As can be observed, the smoothness of the charge data obtained allows a fair use for modelling purposes.

5. Conclusion

A new approximation technique has been developed to construct spline quasi-interpolants of discontinuous data. This has been done by applying the WENO technique to quasi-interpolants defined on non-uniform partitions. The application to academic tests gives excellent results.

Finally, an application of the proposed technique has been presented for real measured data related to memristors fabricated with hafnium oxide as a dielectric. The devices were measured using pulsed input voltage signals, and the current was obtained. The representation of the current data with the quasi-interpolating splines introduced here allows the device charge calculation taking into consideration the non-continuous nature of the experimental data and the non-uniform distribution of the X axis knot set.

CRediT authorship contribution statement

F. Aràndiga: Conceptualization, Investigation. **D. Barrera:** Investigation, Writing – original draft. **S. Eddargani:** Conceptualization, Investigation, Writing – review & editing. **M.J. Ibáñez:** Investigation, Software, Writing – review & editing. **J.B. Roldán:** Data curation, Software.

Acknowledgements

The first author acknowledges the funding provided by the Spanish MINECO project PID2020-117211GB-I00 and GVA project CIAICO/2021/227. The second, fourth and five authors acknowledge project PID2022-139586NB-44 funded by MCIN/AEI/10.13039/501100011033 and by European Union NextGenerationEU/PRTR. The second author also acknowleges the funding by the project QUAL21-011 (Modeling Nature) of the Consejería de Universidad, Investigación e Innovación of the Junta de Andalucía, Spain. The third author is a member of the INdAM Research group GNCS of Italy, and acknowledges the MUR Excellence Department Project awarded to the Department of Mathematics, University of Rome Tor Vergata, CUP E83C23000330006.

* Funding for open access charge: Universidad de Granada / CBUA

References

[1] F.J. Alonso, D. Maldonado, A.M. Aguilera, J.B. Roldan, Memristor variability and stochastic physical properties modeling from a multivariate time series approach, Chaos Solitons Fractals 143 (2021) 110461.

[2] F. Aràndiga, A.M. Belda, Weighted ENO interpolation and applications, Commun. Nonlinear Sci. Numer. Simul. 9 (2004) 187–195.

[3] F. Aràndiga, R. Donat, S.L. Ureña, Nonlinear improvements of quasi-interpolanting splines to approximate piecewise smooth functions, Appl. Math. Comput. 448 (1) (2023) 127946.

[4] F.J. Ariza-López, D. Barrera, S. Eddargani, M.J. Ibáñez, J.F. Reinoso, Spline quasi-interpolation in the Bernstein basis and its application to digital elevation models, Math. Methods Appl. Sci. 46 (2) (2023) 1687–1698.

[5] D. Barrera, C. Dagnino, M.J. Ibáñez, S. Remogna, Point and differential quasi-interpolation on three direction meshes, J. Comput. Appl. Math. 354 (2019) 373–389.
[6] D. Barrera, S. Eddargani, M.J. Ibáñez, S. Remogna, Low-degree spline quasi-interpolants in the Bernstein basis, Appl. Math. Comput. 457 (2023) 128150.
[7] D. Barrera, S. Eddargani, M.J. Ibáñez, S. Remogna, Spline quasi-interpolation in the Bernstein basis on the Powell–Sabin 6-split of a type-1 triangulation, J. Comput. Appl. Math. 424 (2023) 115011.
[8] D. Barrera, M.J. Ibáñez, F. Jiménez-Molinos, A.M. Roldán, J.B. Roldán, A spline quasi-interpolation-based method to obtain the reset voltage in resistive RAMs in the charge-flux domain, J. Comput. Appl. Math. 354 (2019) 326–333.
[9] P. Chen, S. Yu, Compact modeling of RRAM devices and its applications in 1T1R and 1S1R array design, IEEE Trans. Electron Devices 62 (12) (2015) 4022–4028.
[10] O.L. Chua, K.M. Sung, Memristive devices and systems, Proc. IEEE 64 (2) (1976) 209–223.
[11] F. Corinto, P.P. Civalleri, L.O. Chua, A theoretical approach to memristor devices, IEEE J. Emerg. Sel. Top. Circuits Syst. 5 (2) (2015) 123–132.
[12] J.M. Davis, P. Hagelstein, Gibbs phenomena for some classical orthogonal polynomials, J. Math. Anal. Appl. 505 (2022) 125574.
[13] C. de Boor, Splines as linear combinations of B-splines, in: G.G. Lorentz, et al. (Eds.), Approximation Theory II, Academic Press, New York, 1976, pp. 1–47.
[14] S. Eddargani, A. Lamnii, M. Lamnii, On algebraic trigonometric integro splines, Z. Angew. Math. Mech. 100 (2020) e201900262.
[15] S. Eddargani, A. Lamnii, M. Lamnii, D. Sbibih, A. Zidna, Algebraic hyperbolic spline quasi-interpolants and applications, J. Comput. Appl. Math. 347 (2019) 196–209.
[16] G. González-Cordero, M.B. González, H. García, F. Campabadal, S. Dueñas, H. Castán, F. Jiménez-Molinos, J.B. Roldán, A physically based model for resistive memories including a detailed temperature and variability description, Microelectron. Eng. 178 (2017) 26–29.
[17] X. Guan, S. Yu, H.-S. Philip Wong, A SPICE compact model of metal oxide resistive switching memory with variations, Electron Device Lett., IEEE 33 (10) (2012) 1405–1407.
[18] A. Harten, B. Engquist, S. Osher, S. Chakravarthy, Uniformly high order essentially non-oscillatory schemes, III J. Comput. Phys. 71 (1987).
[19] P. Huang, X.Y. Liu, B. Chen, H. Li, Y.J. Wang, Y.X. Deng, J.F. Kang, A physics-based compact model of metal-oxide-based RRAM DC and AC operations, IEEE Trans. Electron Devices 60 (12) (2013) 4090–4097.
[20] P. Huang, D. Zhu, S. Chen, Z. Zhou, Z. Chen, B. Gao, J. Kang, Compact model of HfOX-Based electronic synaptic devices for neuromorphic computing, IEEE Trans. Electron Devices 64 (2) (2017) 614–621.
[21] M.J. Ibáñez, D. Barrera, D. Maldonado, R. Yáñez, J.B. Roldan, Non-uniform spline quasi-interpolation to extract the series resistance in resistive switching memristors for compact modeling purposes, Mathematics 9 (2021) 2159.
[22] M.J. Ibáñez, F. Jiménez-Molinos, J.B. Roldán, R. Yáñez, Estimation of the reset voltage in resistive RAMs using the charge-flux domain and a numerical method based on quasi-interpolation and discrete orthogonal polynomials, Math. Comput. Simulation 164 (2019) 120–130.
[23] D. Ielmini, R. Waser, Resistive Switching: From Fundamentals of Nanoionic Redox Processes to Memristive Device Applications, Wiley-VCH, 2015.
[24] G. Janett, O. Steiner, E.A. Ballester, L. Belluzzi, S. Mishra, A novel fourth-order WENO interpolation technique: A possible new tool designed for radiative transfer, Astron. Astrophys. 624 (2019) 15.
[25] Z. Jiang, Y. Wu, S. Yu, Member, L. Yang, K. Song, Z. Karim, H.-S.P. Wong, A compact model for metal-oxide resistive random access memory with experiment verification, IEEE Trans. Electron Devices 63 (5) (2016) 1884–1892.
[26] M. Lanza, A. Sebastian, W.D. Lu, M. Le Gallo, M.F. Chang, D. Akinwande, F.M. Puglisi, H.N. Alshareef, M. Liu, J.B. Roldan, Memristive technologies for data storage, computation, encryption and radio-frequency communication, Science 376 (6597) (2022) eabj9979, 1–13.
[27] M. Lanza, H.S.P. Wong, E. Pop, D. Ielmini, D. Strukov, B.C. Regan, L. Larcher, M.A. Villena, J.J. Yang, L. Goux, A. Belmonte, Y. Yang, F.M. Puglisi, J. Kang, B. Magyari-Kope, E. Yalon, A. Kenyon, M. Buckwell, A. Mehonic, A. Shluger, H. Li, T.-H. Hou, B. Hudec, D. Akinwande, R. Ge, S. Ambrogio, J.B. Roldan, E. Miranda, J. Suñe, K.L. Pey, X. Wu, N. Raghavan, E. Wu, W.D. Lu, G. Navarro, W. Zhang, H. Wu, R. Li, A. Holleitner, U. Wurstbauer, M. Lemme, M. Liu, S. Long, Q. Liu, H. Lv, A. Padovani, P. Pavan, I. Valov, X. Jing, T. Han, K. Zhu, S. Chen, F. Hui, Y. Shi, Recommended methods to study resistive switching devices, Adv. Electron. Mater. 5 (2019) 1800143.
[28] J.S. Lee, S. Lee, T.W. Noh, Resistive switching phenomena: A review of statistical physics approaches, Appl. Phys. Rev. 2 (2015) 031303.
[29] D. Maldonado, S. Aldana, M.B. González, F. Jiménez-Molinos, F. Campabadal, J.B. Roldán, Parameter extraction techniques for the analysis and modeling of resistive memories, Microelectron. Eng. 265 (2022) 111876.
[30] D. Maldonado, S. Aldana, M.B. González, F. Jiménez-Molinos, M.J. Ibáñez, D. Barrera, F. Campabadal, J.B. Roldán, Variability estimation in resistive switching devices, a numerical and kinetic monte carlo perspective, Microelectron. Eng. 257 (2022) 111736.
[31] M.L. Mazure, Blossoms and optimal bases, Adv. Comput. Math. 20 (2004) 177–203.
[32] F. Pan, S. Gao, C. Chen, C. Song, F. Zeng, Recent progress in resistive random access memories: Materials, switching mechanisms and performance, Mater. Sci. Eng. 83 (2014) 1–59.
[33] R. Picos, J.B. Roldán, M.M. Al Chawa, P. García-Fernández, F. Jiménez-Molinos, E. García-Moreno, Semiempirical modeling of reset transitions in unipolar resistive-switching based memristors, Radioeng. J. 24 (2015) 420–424.
[34] S. Poblador, M. Maestro-Izquierdo, M. Zabala, M.B. González, F. Campabadal, Methodology for the characterization and observation of filamentary spots in HfOx-based memristor devices, Microelectron. Eng. 223 (2020) 111232.
[35] J.B. Roldán, F.J. Alonso, A.M. Aguilera, D. Maldonado, M. Lanza, Time series statistical analysis: A powerful tool to evaluate the variability of resistive switching memories, J. Appl. Phys. 125 (2019) 174504.
[36] J.B. Roldán, G. González-Cordero, R. Picos, E. Miranda, F. Palumbo, F. Jiménez-Molinos, E. Moreno, D. Maldonado, S.B. Baldomá, M. Moner Al Chawa, C. de Benito, S.G. Stavrinides, J. Suñé, L.O. Chua, On the thermal models for resistive random access memory circuit simulation, Nanomaterials 11 (2021) 1261.
[37] P. Sablonnière, D. Sbibih, Integral spline operators exact on polynomials, Approx. Theory Appl. 10 (1994) 56–73.
[38] P. Sablonnière, D. Sbibih, M. Tahrichi, High-order quadrature rules based on spline quasi-interpolants and application to integral equations, Appl. Numer. Math. 62 (2012) 507–520.
[39] I.J. Schoenberg, Contributions to the problem of approximation of equidistant data by analytic functions. Part A. On the problem of smoothing or graduation. A first class of analytic approximation formulae, Quart. Appl. Math. 4 (1946) 45–99.
[40] I.J. Schoenberg, Contributions to the problem of approximation of equidistant data by analytic functions. Part B. On the problem of osculatory interpolation, a second class of analytic approximation formulae, Quart. Appl. Math. 4 (1946) 112–141.
[41] J. Shi, C. Hu, C. Shu, A technique of treating negative weights in WENO schemes, J. Comput. Phys. 175 (2002) 108–127.
[42] H. Socas-Navarro, J.T. Bueno, R.B. Cobo, Non-LTE inversion of Stokes profiles induced by the Zeeman effect, Astrophys. J. (2000).
[43] T. Sorokina, F. Zeilfelder, An explicit quasi-interpolation scheme based on C^1 quartic splines on type-1 triangulations, Comput. Aided Geom. Design 25 (2008) 1–13.
[44] S. Spiga, A. Sebastian, D. Querlioz, B. Rajendran, Memristive Devices for Brain-Inspired Computing, Elsevier, 2020.
[45] C. Wu. L. Wu. H. Li, S. Zhang, Very high order WENO schemes using efficient smoothness indicators, J. Comput. Phys. 432 (2021) 110158.